nature photonics

REVIEW ARTICLE

PUBLISHED ONLINE: 26 OCTOBER 2014 | DOI: 10.1038/NPHOTON.2014.248

Topological photonics

Ling Lu*, John D. Joannopoulos and Marin Soljačić

The application of topology, the mathematics of conserved properties under continuous deformations, is creating a range of new opportunities throughout photonics. This field was inspired by the discovery of topological insulators, in which interfacial electrons transport without dissipation, even in the presence of impurities. Similarly, the use of carefully designed wavevector-space topologies allows the creation of interfaces that support new states of light with useful and interesting properties. In particular, this suggests unidirectional waveguides that allow light to flow around large imperfections without back-reflection. This Review explains the underlying principles and highlights how topological effects can be realized in photonic crystals, coupled resonators, metamaterials and quasicrystals.

Frequency, wavevector, polarization and phase are degrees of freedom that are often used to describe a photonic system. Over the past few years, topology — a property of a photonic material that characterizes the quantized global behaviour of the wavefunctions on its entire dispersion band — has emerged as another indispensable degree of freedom, thus opening a path towards the discovery of fundamentally new states of light and possible revolutionary applications. Potential practical applications of topological photonics include photonic circuitry that is less dependent on isolators and slow light that is insensitive to disorder.

Topological ideas in photonics branch from exciting developments in solid-state materials, along with the discovery of new phases of matter called topological insulators[1,2]. Topological insulators, being insulating in the bulk, conduct electricity on their surface without dissipation or back-scattering, even in the presence of large impurities. The first example of this was the integer quantum Hall effect, discovered in 1980. In quantum Hall states, two-dimensional (2D) electrons in a uniform magnetic field form quantized cyclotron orbits of discrete energies called Landau levels. When the electron energy sits within the energy gap between the Landau levels, the measured edge conductance remains constant within an accuracy of around one part in a billion, regardless of sample size, composition and purity. In 1988, Haldane proposed a theoretical model for achieving the same phenomenon in a periodic system without Landau levels[3] — the quantum anomalous Hall effect.

In 2005, Haldane and Raghu transferred the key feature of this electronic model to the realm of photonics[4,5]. They theoretically proposed the photonic analogue of the quantum (anomalous) Hall effect in photonic crystals[6] (the periodic variation of optical materials that affects photons in the same manner as solids modulate electrons). Three years later, this idea was confirmed by Wang *et al.*, who provided realistic material designs[7] and experimental observations[8]. These studies spurred numerous subsequent theoretical[9–13] and experimental investigations[14–16].

In ordinary waveguides, back-reflection is a major source of unwanted feedback and loss that hinders large-scale optical integration. The works cited above demonstrate that unidirectional edge waveguides transmit electromagnetic waves without back-reflection even in the presence of arbitrarily large disorder. This is an ideal transport property that is unprecedented in photonics. Topological photonics promises to offer unique, robust designs and new device functionalities for photonic systems by providing immunity to performance degradation induced by fabrication imperfections or environmental changes.

In this Review, we present the key concepts, experiments and proposals in the field of topological photonics. Starting with an introduction to the relevant topological concepts, we introduce the 2D quantum Hall phase through the stability of Dirac cones[4,5], followed by its realizations in gyromagnetic photonic crystals[7,8,13], coupled resonators[9,10,16] and waveguides[15], bianisotropic metamaterials[11] and quasicrystals[14]. We then extend our discussion to three dimensions, wherein we describe the stability of line nodes and Weyl points and their associated surface states[12]. We conclude by considering the outlook for further theoretical and technological advances.

Topological phase transition

Topology is the branch of mathematics concerned with quantities that are preserved under continuous deformations. For example, the six objects in Fig. 1a all have different geometries, but there are only three different topologies. The sphere can be continuously changes into the spoon, so they are topologically equivalent. The torus and coffee cup are also topologically equivalent, and so too are the double torus and tea pot. Different topologies can be mathematically characterized by integers called topological invariants — quantities that remain constant under arbitrary continuous deformations of the system. For the above closed surfaces, the topological invariant is its genus, which corresponds to the number of holes within a closed surface. Objects with the same topological invariant are topologically equivalent; that is, they are in the same topological phase. Only when a hole is created or removed in the object does the topological invariant change. This process is known as a topological phase transition.

Topologies for material systems in photonics are defined on the dispersion bands in reciprocal (wavevector) space. The topological invariant of a 2D dispersion band is the Chern number (C, Box 1), a quantity that characterizes the quantized collective behaviour of the wavefunctions on the band. Once a physical observable can be written as a topological invariant, it changes only discretely; thus, it will not respond to continuous small perturbations. These perturbations can be arbitrary continuous changes in the system parameters.

Optical mirrors reflect light of a given frequency range, due to the lack of available optical states inside the mirror. Thus, the frequency gaps of a mirror are analogous to the energy gaps of an insulator. The sum of the Chern numbers of the dispersion bands below the frequency gap indicates the topology of the mirror. This can be understood as the total number of 'twists' and 'untwists' of the system up to the gap frequency. Ordinary mirrors like air (total internal reflection), metal or Bragg reflectors all have zero Chern

Department of Physics, Massachusetts Institute of Technology, Cambridge, Massachusetts 02139, USA. *e-mail: linglu@mit.edu

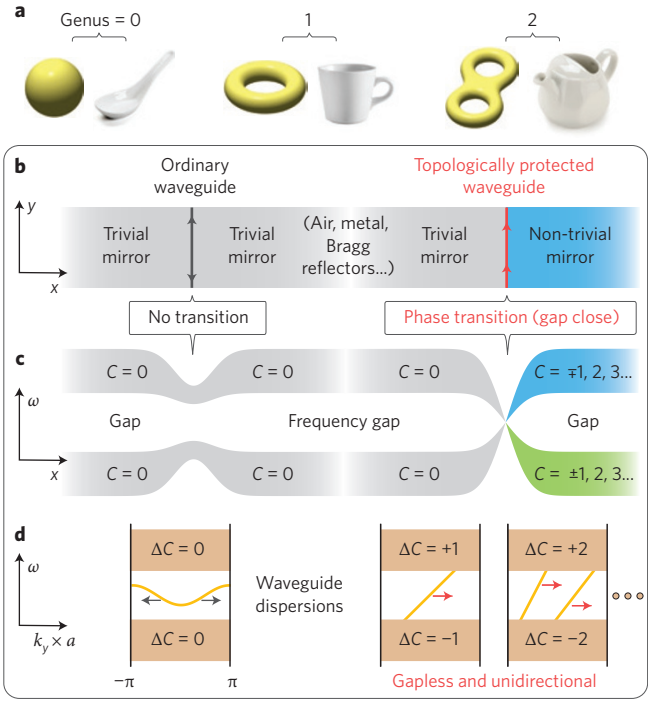

Figure 1 | Topological phase transition. a, Six objects of different geometries can be grouped into three pairs of topologies. Each pair has the same topological invariant, known as its genus. **b**, Two waveguides formed by mirrors of different (right) and same (left) topologies. **c**, Frequency bands of different topologies cannot transition into each other without closing the frequency gap. A topological phase transition takes place on the right, but not on the left. **d**, Interfacial states have different connectivity with the bulk bands, depending on the band topologies of the bulk mirrors. Here, a is the period of the waveguide propagating along y, and ΔC is the change in Chern number between the corresponding bulk bands on the right and left of the waveguide. The magnitude of ΔC equals the number of gapless interfacial modes and the sign of ΔC indicates the direction of propagation.

numbers, which makes them topologically trivial. Mirrors with non-zero Chern numbers are topologically non-trivial.

The most fascinating and peculiar phenomena take place at the interface between two mirrors with different topological invariants. The edge waveguide formed by these two topologically inequivalent mirrors (Fig. 1b, right) is topologically distinct from an ordinary waveguide, which is formed between topologically equivalent mirrors (Fig. 1b, left). The distinction lies in the frequency spectra of their edge modes inside the bulk frequency gap. On the left of Fig. 1c, the two frequency bands both have zero Chern numbers, so they can directly connect across the interface without closing the frequency gap. However, when the two mirrors have different Chern numbers, topology does not allow them to connect to each other directly. A topological phase transition must take place at the interface: this requires it to close the frequency gap, neutralize the Chern numbers, then reopen the gap. This phase transition (Fig. 1c, right), ensures gapless frequency states at the interface: there must exist edge states at all frequencies within the gap of the bulk mirrors. The gapless spectra of the edge states are topologically protected; that is, their existence is guaranteed by the difference of the topologies of the bulk materials on the two sides. In general, the number of gapless edge modes equals the difference of the bulk topological invariants across the interface. This is known as the bulk-edge correspondence.

The topological protection of edge waveguides can also be understood in reciprocal space. Figure 1d shows the dispersion diagrams of both ordinary (left) and gapless (right) waveguides. On the left, the ordinary waveguide dispersion is disconnected from the bulk bands and can be continuously moved out of the frequency gap into the bulk bands. On the right, however, the gapless waveguide dispersion connects the bulk frequency bands above and below the frequency gap. It cannot be moved out of the gap by changing the edge terminations. Similar comparisons between the edge band diagrams are shown in Fig. 2. The only way to alter these connectivities is through a topological phase transition; that is, closing and reopening the bulk frequency gap.

The unidirectionality of the protected waveguide modes can be seen from the slopes (group velocities) of the waveguide dispersions. An ordinary waveguide (Fig. 1d, left) supports bidirectional modes because it back-scatters at imperfections. In contrast, a topologically protected gapless waveguide (Fig. 1d, right) is unidirectional as it has only positive (or only negative) group velocities. In addition, there are no counter-propagating modes at the same frequencies as the one-way edge modes. This enables light to flow around imperfections with perfect transmission — the light can only go forwards. The operating bandwidth of such a one-way waveguide is as large as the size of the bulk frequency gap.

From Dirac cones to quantum Hall topological phase

One effective approach for finding non-trivial mirrors (frequency gaps with non-zero Chern numbers) is to identify the phase transition boundaries of the system in the topological phase diagram, where the bulk frequency spectrum is gapless. Correct tuning of the system parameters thus open gaps that belong to different topological phases. In 2D periodic systems, these phase boundaries are point-degeneracies in the bandstructure. The most fundamental 2D point degeneracy is a pair of Dirac cones with linear dispersions between two bands. In three dimensions, the degeneracies involve line nodes and Weyl points, which we will discuss later in this Review.

Dirac cones are protected, in the entire 2D Brillouin zone, by by 'PT symmetry', which is the product of time-reversal symmetry (T, Box 2) and parity (P) inversion. Every Dirac cone has a quantized Berry phase (Box 1) of π looped around it[17,18]. Protected Dirac cones generate and annihilate in pairs[19–23]. The effective Hamiltonian close to a Dirac point in the x–y plane can be expressed by $H(\mathbf{k}) = v_x k_x \sigma_x + v_y k_y \sigma_z$, where v_i are the group velocities and σ_i are the Pauli matrices. Diagonalization leads to the solution $\omega(\mathbf{k}) = \pm\sqrt{(v_x^2 k_x^2 + v_y^2 k_y^2)}$. Although both P and T map the Hamiltonian from $\mathbf{k}$ to $-\mathbf{k}$, they differ by a complex conjugation: $(PT)\ H(\mathbf{k})\ (PT)^{-1} = H(\mathbf{k})^*$. PT symmetry requires the Hamiltonian to be real and thus absent of σ_y, which is imaginary. A 2D Dirac point-degeneracy can be lifted by any perturbation that is proportional to σ_y in the Hamiltonian or, equivalently, by any perturbation that breaks PT. Therefore, breaking either P or T will open a bandgap between the two bands.

However, the bandgaps opened by breaking P[24] and T individually are topologically inequivalent[5,25], as the bulk bands in these two cases carry different Chern numbers. The Chern number is the integration of the Berry curvature ($\mathcal{F}(\mathbf{k})$ in Table B1) on a closed surface in wavevector space. $\mathcal{F}(\mathbf{k})$ is a pseudovector that is odd under T but even under P. In the presence of both P and T, $\mathcal{F}(\mathbf{k}) = 0$. When either P or T is broken, the Dirac cones open and each degeneracy-lifting contributes a Berry flux of magnitude π to each of the bulk bands. In the presence of T (P broken), $\mathcal{F}(\mathbf{k}) = -\mathcal{F}(-\mathbf{k})$. The Berry flux contributed by one pair of Dirac points at $\mathbf{k}$ and $-\mathbf{k}$ are of opposite signs. Integration over the whole 2D Brillouin zone always equals zero, and thus so do the Chern numbers. In contrast, in the presence of P (T broken), $\mathcal{F}(\mathbf{k}) = \mathcal{F}(-\mathbf{k})$. Here, the total Berry flux adds up to 2π and the Chern number equals one. More pairs of Dirac cones can lead to higher Chern numbers[13]. This T-breaking 2D quantum Hall topological phase is shown in red in the phase diagram of Fig. 2.

Box 1 | Topological invariant.

A closed surface can be smoothly deformed into various geometries without cutting and pasting. The Gauss–Bonnet theorem[92] of equation (1) below, which connects geometry to topology, states that the total Gaussian curvatures ($\mathcal{K}$) of a 2D closed surface is always an integer. This topological invariant, named genus (g), characterizes the topology of the surface; that is, the number of holes within. Examples of surfaces with different geni are shown in Fig. 1a.

$$\frac{1}{2\pi}\int_{\text{surface}} \mathcal{K}dA = 2(1-g) \quad (1)$$

A two dimensional Brillouin zone is also a closed surface with the same topology of a torus due to its periodic boundary conditions (Fig. B1). Table B1 lists the definitions[93] of Berry curvature and Berry flux with respect to Bloch wavefunctions in the Brillouin zone by comparing them to the familiar case of magnetic field and magnetic flux in real space. Integrating the Berry curvature over the torus surface yields the topological invariant known as the 'Chern number', which gives a measure of the total quantized Berry flux of the 2D surface. The Chern number can be viewed as the number of monopoles of Berry flux inside a closed surface, as illustrated in Fig. B1. An efficient way to calculate Chern numbers in discretized Brillouin zones is described in ref. 94.

Topological invariants can be arbitrary integers ($\mathbb{Z}$) or binary numbers ($\mathbb{Z}_2$, meaning $\mathbb{Z}$ mod 2). Chern numbers are integers ($C \in \mathbb{Z}$) and the sum of the Chern numbers over all bands of a given system is zero.

Historically, the geometric phase was first discovered in optics by Pancharatnam[95] prior to the discovery of the Berry phase[96]. The first experiments demonstrating the Berry phase were performed in optical fibres[97].

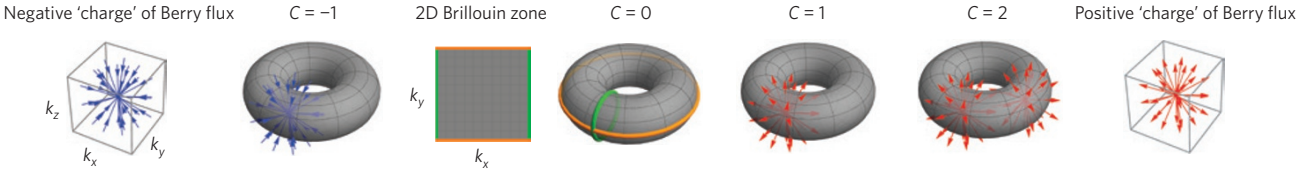

Figure B1 | Chern number as the number of Berry monopoles in momentum space. A 2D Brillouin zone is topologically equivalent to a torus. The Chern number (C) can be viewed as the number of monopoles (charges) of Berry flux inside a closed 2D surface. The arrows represent Berry curvature from the positive and negative charges. In a 3D Brillouin zone, these monopoles are Weyl points.

Table B1 | Comparison of the Berry phase for Bloch wavefunctions and the Aharonov–Bohm phase.

Vector potential	$\mathbf{A}(\mathbf{r})$	$\mathcal{A}(\mathbf{k}) = \langle u(\mathbf{k})\|i\nabla_{\mathbf{k}}\|u(\mathbf{k})\rangle$	Berry connection
Aharonov–Bohm phase	$\oint \mathbf{A}(\mathbf{r})\cdot d\mathbf{l}$	$\oint \mathcal{A}(\mathbf{k})\cdot d\mathbf{l}$	Berry phase
Magnetic field	$\mathbf{B}(\mathbf{r}) = \nabla_{\mathbf{r}}\times\mathbf{A}(\mathbf{r})$	$\mathcal{F}(\mathbf{k}) = \nabla_{\mathbf{k}}\times\mathcal{A}(\mathbf{k})$	Berry curvature
Magnetic flux	$\iint \mathbf{B}(\mathbf{r})\cdot d\mathbf{s}$	$\iint \mathcal{F}(\mathbf{k})\cdot d\mathbf{s}$	Berry flux
Magnetic monopoles	$\# = \frac{e}{h}\oiint \mathbf{B}(\mathbf{r})\cdot d\mathbf{s}$	$C = \frac{1}{2\pi}\oiint \mathcal{F}(\mathbf{k})\cdot d\mathbf{s}$	Chern number

The Berry connection measures the local change in phase of wavefunctions in momentum space, where $i\nabla_{\mathbf{k}}$ is a Hermitian operator. Similar to the vector potential and Aharonov–Bohm phase, Berry connection and Berry phase are gauge dependent (that is, $u(\mathbf{k}) \to e^{i\phi(\mathbf{k})}u(\mathbf{k})$). The rest of the quantities are gauge-invariant. The Berry phase is defined only up to multiples of 2π. The phase and flux can be connected through Stokes' theorem. Here, $u(\mathbf{k})$ is the spatially periodic part of the Bloch function; the inner product of $\langle\rangle$ is done in real space. The one-dimensional Berry phase is also known as the Zak phase.

Gyromagnetic photonic crystals

Wang *et al.* were the first to realize the photonic analogue of the quantum Hall effect at microwave frequencies[8]. Their experiment broke T by applying a uniform magnetic field on gyromagnetic photonic crystals, resulting in a single topologically protected edge mode that propagated around arbitrary disorder without reflection.

Such single-mode one-way waveguides can be realized in coupled defect cavities[26], self-guide[27] in free-standing slabs[28] and have a robust local density of states[29]. They have enabled novel device designs for tunable delays and phase shifts with unity transmission[7], reflectionless waveguide bends and splitters[30], signal switches[31], directional filters[32,33], broadband circulators[34] and slow-light waveguides[35]. Very recently, multimode one-way waveguides of large bulk Chern numbers ($|C| = 2, 3, 4$) have been theoretically discovered by opening gaps of multiple point degeneracies simultaneously[13], thus providing even richer possibilities in terms of device functionalities.

Wang *et al.* based their experiments[8] on a 2D square lattice photonic crystal comprising an array of gyromagnetic ferrite rods confined vertically between two metallic plates to mimic the 2D transverse magnetic (TM) modes. They also added a metal wall to the surrounding edges to prevent radiation loss into air (Fig. 3a). Without the external magnetic field, the second and third TM bands are connected by a quadratic point-degeneracy comprising a pair of Dirac cones[36]. Under a uniform static magnetic field (0.2 T) that breaks T, anti-symmetric imaginary off-diagonal terms develop in the magnetic permeability tensor (μ). The quadratic degeneracy breaks and a complete bandgap forms between the second and third bands, which both have non-zero Chern numbers. The red dispersion line in Fig. 3b is the gapless edge state inside the second bandgap, which has only positive group velocities at around 4.5 GHz. Numerical simulation results (Fig. 3c, top) verified that an antenna inside the waveguide can only emit in the forward direction in the bulk frequency gap. The experimental transmission data in Fig. 3d shows that the backwards reflection is more than five orders of magnitude smaller than the forwards transmission after propagating over only eight lattice periods. More importantly, there is no increase in the reflection amplitude even after the insertion of large metallic scatterers (Fig. 3c, bottom). Indeed, new one-way edge modes automatically form wherever a new interface is created, thus providing a path for light to circumvent the scatter. This is precisely

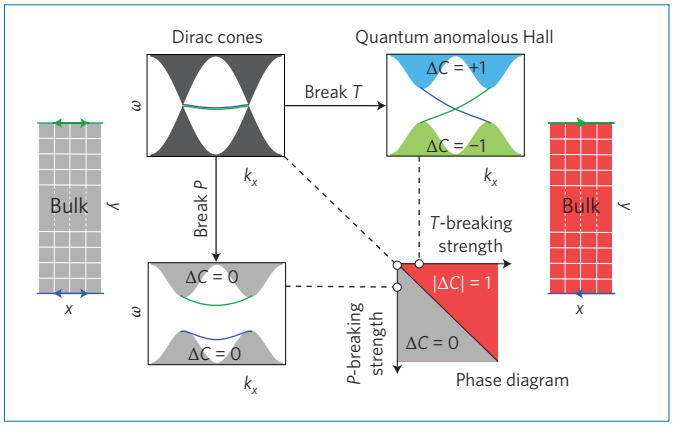

Figure 2 | Topological phase diagram of the 2D quantum Hall phase. The top-left image shows a band diagram of edge states in which the bulk dispersions form a pair of Dirac cones (grey) protected by *PT* symmetry. The green and blue lines represent edge dispersions on the top and bottom edges. When either *P* or *T* are broken, a bandgap can form in the bulk but not necessarily on the edges. When *T*-breaking is dominant, the two bulk bands split and acquire Chern numbers of ±1. Thus, there exists one gapless edge dispersion on each of the top and bottom interfaces, assuming the bulk is interfaced with topologically trivial mirrors. This *T*-breaking phase of non-zero Chern numbers is the quantum Hall phase, plotted in red in the phase diagram.

the topological protection provided by the bulk of a photonic crystal that contains non-zero Chern numbers.

There are other types of one-way waveguides that break *T* (ref. 37), but these are not protected by topology. In general, magnetic responses are very weak in optical materials. Realization at optical frequencies therefore remains a challenge.

Coupled resonators

Photons in an array of coupled resonators are similar to electrons in an array of atoms in solids. The photon couplings between the resonators can be controlled to form topologically non-trivial frequency gaps with robust edge states. Researchers obtained the photonic analogues of the integer quantum Hall effect by constructing both static and time-harmonic couplings that simulate the electron's behaviour in a uniform magnetic field. When the *T*-breaking is implemented by accurate time-harmonic modulations, unidirectional edge waveguides immune to disorder can be realized at optical frequencies.

In electronic systems, the first quantum Hall effect was observed in a 2D electron gas subject to an out-of-plane magnetic field. As illustrated in Fig. 4a, the bulk electrons undergo localized cyclotron motions, while the unidirectional edge electrons have an extended wavefunction. Again, the number of gapless edge channels equals the Chern number of the system. Here, the physical quantity describing the magnetic field is the vector potential, which can be written in the form $\mathbf{A} = By\hat{\mathbf{x}}$. An electron accumulates an Aharonov–Bohm (AB) phase of

$$\phi = \oint \mathbf{A}(\mathbf{r}) \cdot \mathrm{d}\mathbf{l}$$

after a closed loop (see Table B1). An electron going against the cyclotron motion acquires a phase of $-\phi$ (dotted circle in Fig. 4a), so it has a different energy (from the electrons moving in solid circles). The spin degeneracy of electrons is lifted by Zeeman splitting.

Although a photon does not interact with a magnetic field, it does acquire a phase change after passing through a closed loop. By carefully tuning the propagation and coupling phases, Hafezi *et al.* designed[9] a lattice of optical resonators in which the photons acquire the same phase as the AB phase of electrons moving in a uniform magnetic field. This is different from a true quantum Hall topological phase, as *T* is not broken in their static and reciprocal resonator array. Thus, back-reflections are allowed because time-reversed channels always exist at the same frequencies. Nevertheless, Hafezi *et al.* were able to observe the edge states at near-infrared (1.55 μm) wavelengths in the first set of experiments performed on a silicon-on-insulator platform[16], and in a recent experiment[38] also showed that robustness against particular types of disorder can still be achieved owing to the topological features of the phase arrangements.

Box 2 | Time reversal symmetry.

Symmetry considerations are crucial when determining the possible topological phases of a system. For example, the quantum Hall phase requires the breaking of time-reversal symmetry (*T*). On the other hand, in the recently discovered 2D and 3D topological insulators in electronics, *T*-symmetry is required to protect these topological phases characterized by $\mathbb{Z}_2$ topological invariants. For example, the 2D topological insulator, also known as the quantum spin Hall effect[98], allows the coexistence of counter-propagating spin-polarized gapless edge states. Without *T*-symmetry, however, these edge states can scatter into each other. The edge energy spectrum opens a gap and the insulator can continuously connect to trivial insulators, such as the vacuum. A large table of symmetry-protected topological phases have been theoretically classified[73,74]. These systems have robust interfacial states that are topologically protected only when the corresponding symmetries are present[75].

Here we point out the fundamental difference in time-reversal symmetry between electrons and photons. A photon is a neutral non-conserved non-interacting spin-1 Boson that satisfies Maxwell's equations, whereas an electron is a charged conserved interacting spin-1 Fermion that satisfies Schrödinger's equation. Similar to Schrödinger's equation, the lossless Maxwell's equations at non-zero frequencies can be written as a generalized Hermitian eigenvalue problem:

$$i\begin{pmatrix} 0 & \nabla\times \\ -\nabla\times & 0 \end{pmatrix}\begin{pmatrix} \mathbf{E} \\ \mathbf{H} \end{pmatrix} = \omega\begin{pmatrix} \epsilon & \chi \\ \chi^{\dagger} & \mu \end{pmatrix}\begin{pmatrix} \mathbf{E} \\ \mathbf{H} \end{pmatrix}$$

where $\varepsilon^{\dagger} = \varepsilon$, $\mu^{\dagger} = \mu$ and χ is the bianisotropy term, where † is Hermitian conjugation.

The anti-unitary time *T* operator is given by:

$$\begin{pmatrix} 1 & 0 \\ 0 & -1 \end{pmatrix} K$$

which squares to unity, where *K* is complex conjugation (*). When $\varepsilon^{*} = \varepsilon$, $\mu^{*} = \mu$ and $\chi = -\chi^{*}$, the system is *T*-invariant. Rotating the spin by 2π is the same as applying the *T* operator twice (T^2). But T^2 has different eigenvalues for photons ($T^2 = +1$) and electrons ($T^2 = -1$). It is this minus sign that ensures Kramer's degeneracies for electrons at *T*-invariant $\mathbf{k}$ points in the Brillouin zone, thus providing the possibility of gapless connectivity for edge dispersions in the bulk gap. This fundamental distinction results in different topological classifications for photons and electrons with respect to *T*. For example, photons do not have the same topological phases of 2D or 3D topological insulators protected by *T* as for electrons.

Figure 4b shows a 2D array of whispering-gallery resonators that are spatially coupled by the waveguides between. Each resonator has two whispering-gallery modes that propagate clockwise (green) and counter-clockwise (red). They are time-reversed pairs and are similar to the 'spin-up' and 'spin-down' degrees of freedom for electrons. The lengths of the coupling waveguides are carefully designed so that the total coupling phase between resonators precisely matches the AB phase in Fig. 4a: the vertical couplings have no phase changes, whereas the horizontal couplings have phases that are linear in y. In each 'spin' space, photons of opposite circulations experience opposite 'AB' phases ($\pm\phi$), just like the electrons in Fig. 4a. These opposite loops are also illustrated in solid and dashed red lines for the 'spin-up' photons in Fig. 4b. As a result, the photonic frequency spectrum in this resonator array[39,40] exhibits both Landau levels and fractal patterns known as the Hofstadter butterfly, which are the signatures of a 2D electron in a uniform magnetic field — the integer quantum Hall effect. However, without breaking T, the two copies of 'spin' spaces are degenerate in frequency and couple to each other. Only by assuming that these two 'spins' decouple from each other completely can Chern numbers of the same magnitude but opposite sign be defined and potentially measured[41] in each 'spin' space. (The 'spin'-polarized counter-propagating edge modes bear similarities to the edge currents in the quantum spin Hall effect for electrons, but they are fundamentally different in symmetry protections and topological invariants, as discussed in Box 2.) These photonic gapless edge modes are robust against disorder that does not induce 'spin' flips. For example, when a defect edge resonator has a different size and resonance frequency from the bulk resonators, then the edge mode will find another route to pass around this defect resonator. A recent study[42,43] suggested that the required spatially varying couplers along y can be made identical and periodic, but still achieving the same phenomena. Unfortunately, in these reciprocal schemes, perturbations that induce 'spin' flips are practically ubiquitous: local fabrication imperfections on the resonators or the couplers and even the coupling processes themselves can mix the 'spins' and induce back-scattering.

Back-scattering in the above time-reversal-invariant systems can be eliminated by breaking T, for example using spatially coherent time-domain modulations, as proposed theoretically in ref. 10. Fang *et al.* propose placing two kinds of single-mode resonators in the lattice shown in Fig. 4c. When the nearest-neighbour coupling is dominant, the two resonators (which have different resonance frequencies) can couple only through the time-harmonic modulation between them. The vertical coupling phases are zero and the horizontal coupling phases increase linearly along y, thereby producing effective AB phases from a uniform magnetic field. Photons moving in opposite directions have opposite phases, so they have different frequencies. Floquet's theorem in the time domain — similar to Bloch's theorem in the spatial domain — is used to solve this lattice system of time-periodic modulations. The resulting Floquet bandstructure has the same gapless edge states as that of a static quantum Hall phase.

Achieving accurate and coherent time-harmonic modulations for a large number of resonators is experimentally challenging towards optical frequencies[44–46]. By translating the modulation from the time domain to the spatial domain, Rechtsman *et al.* experimentally demonstrated the photonic analogue of the quantum Hall effect using optical photons (633 nm)[15]. These are also the first experiments on Floquet topological phases[47,48]. Starting with a 2D resonator array (Fig. 4d), the researchers extended the cavities along z to give a periodic array of coupled waveguides propagating in this direction. In their system, z plays the role of time. More specifically, the paraxial approximation of Maxwell's equations results in an equation governing diffraction (propagating in z) that is equivalent to Schrödinger's equation evolving in time. The periodic helical modulations[49,50] in z break the z-symmetry, which is equivalent to the time-domain modulations that break T. This symmetry-breaking opens up protected band degeneracies in the Floquet bandstructure, thus forming a topologically non-trivial bandgap that contains protected gapless edge modes.

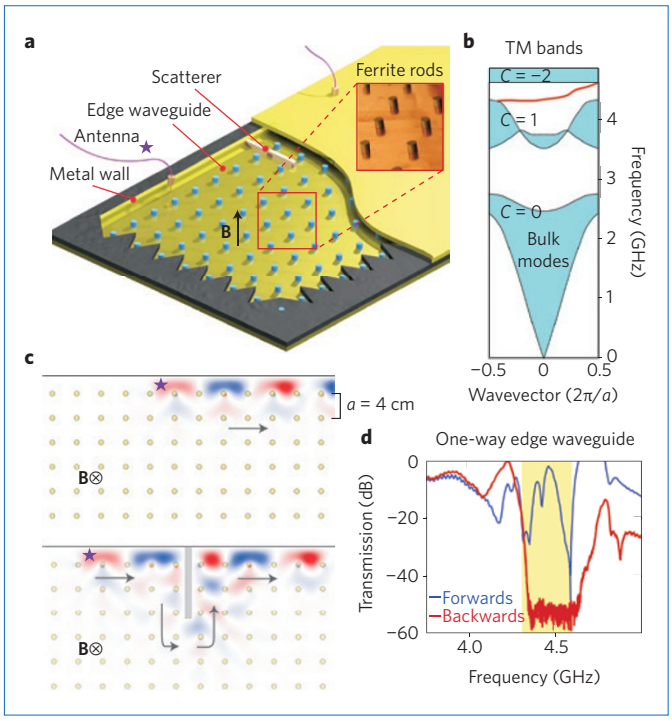

Figure 3 | First experimental demonstration of the topologically protected one-way edge waveguide at microwave frequencies. **a**, Experimental set-up for measuring the one-way edge state between the metal wall and the gyromagnetic photonic crystal confined between the metallic plates to mimic the 2D TM modes. The inset is a picture of the ferrite rods that constitute the photonic crystal of lattice period $a = 4$ cm. **b**, The bandstructure of the one-way gapless edge state between the second and third bands of non-zero Chern numbers. **c**, Simulated field propagation of the one-way mode and its topological protection against a long metallic scatterer. **d**, The measured robust one-way transmission data of the edge waveguide.

The idea of creating effective magnetic fields for neutral particles[51] using synthetic gauge fields was first explored in optical lattices[52]. Very recently, similar gauge fields have also been studied in optomechanics[53] and radiofrequency circuits[54]. Finally, although approximations such as 'nearest-neighbour in space' or 'rotating-wave in time' were adopted through the analysis of the systems described in this section, these higher order corrections do not fundamentally alter the topological invariants and phenomena demonstrated.

Bianisotropic metamaterials

In bianisotropic materials ($\chi \neq 0$, Box 2)[55], the coupling between electric and magnetic fields provides a wider parameter space for the realization of different topological phases. In particular, it has been shown that bianisotropic photonic crystals can achieve topological phases without breaking T (T-invariant); thus, neither magnetism nor time-domain modulations are needed for the topological protection of edge states. Bianisotropic responses are known as 'optical activity' in chiral molecules and can also be designed in metamaterials.

Bianisotropy acts on photons in a similar way to how spin-orbit coupling acts on electrons[56]. In their inspiring theoretical proposal[11], Khanikaev *et al.* enforced polarization ('spin') degeneracy for photons by equating ε to μ ($\varepsilon = \mu$), so that the transverse electric (TE) and TM modes in two dimensions are exactly degenerate in frequencies.

When the pseudo-tensor χ is of the same form as the gyroelectric or gyromagnetic terms in ε or μ, then χ acts as a magnetic field on each polarization with opposite signs, without breaking T. This system can be separated into two independent 'spin' subspaces, in which quantum anomalous Hall phases exist with opposite Chern numbers.

Very recently, it was suggested that the $\varepsilon = \mu$ condition could potentially be relaxed[57]. Indeed, in their experimental work, Chen *et al.*[58] relaxed the material requirements for matching ε and μ. They also realized a broadband effective bianisotropic response by embedding the ε/μ-matched metamaterials in a metallic planar waveguide. These advances enabled them to observe the 'spin-polarized' edge transport at around 3 GHz.

Similar to the T-invariant resonator arrays in Fig. 4b and refs 9,16,38,42,43, the above metamaterial realizations also require strict conditions in order to decouple the two copies of 'spins'. In these cases, the requirements are on the accurate realization of the constitutive parameters during metamaterial manufacturing. The lack of intrinsic T-protected quantum spin Hall topological phase is one of the most fundamental differences between electronic and photonic systems, as discussed in Box 2. Finally, gapless surface states were also proposed to exist in a bulk hyperbolic metamaterial that exhibits bianisotropic responses[59].

Quasicrystals

Quasicrystals are aperiodic structures that possess spatial order. They also have frequency gaps and interfacial states. Quasicrystals can be constructed from the projections of periodic crystals in higher dimensions. Krauss *et al.*[14] projected the 2D quantum Hall phase onto a 1D quasicrystal model containing a tunable parameter that is equivalent to the Bloch wavevector lost during the projection. Scanning this periodic parameter reproduced the full gapless frequency spectrum of the 2D quantum Hall phase; that is, the 0D edge mode frequency of the 1D quasicrystal continuously swept through the 1D bulk gap. The researchers fabricated 1D optical waveguide arrays to be spatially varying along z according to the continuous tuning of this parameter. In their system, z plays the role of time. They observed the edge state start from one edge of the waveguide array, merge into the bulk modes, then switch to the other edge of the array. Thus, light is adiabatically transferred in space from edge to edge. Going a step further, they proposed the potential realization of the quantum Hall phase in 4D using 2D quasicrystals[60].

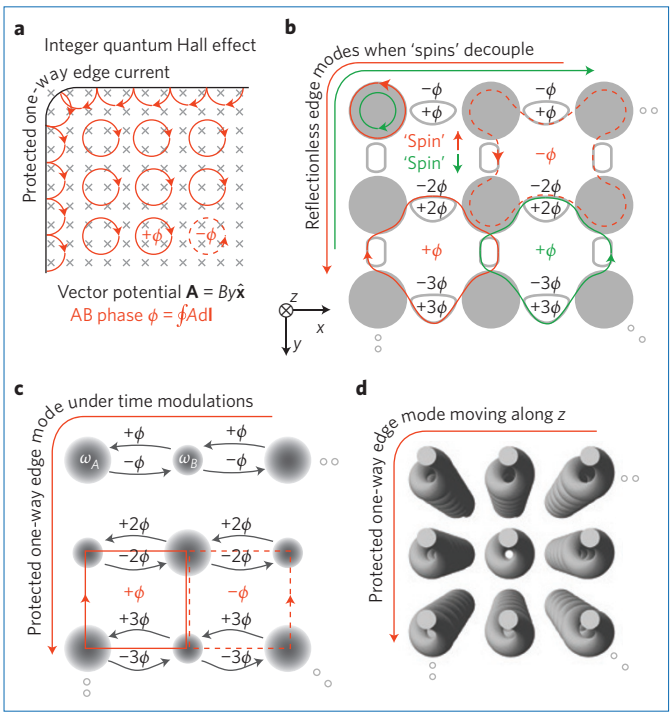

Figure 4 | Quantum Hall phase of electrons in a magnetic field and of photons in coupled resonators exhibiting an effective magnetic field. **a**, Cyclotron motions of electrons in a static magnetic field ($B\hat{\mathbf{z}}$). The vector potential increases linearly in y. **b**, A 2D lattice of photonic whispering-gallery resonators coupled through static waveguides. The horizontal coupling phases increase linearly in y. The two 'spins' of the whispering-gallery resonators are degenerate in the effective magnetic field. **c**, A 2D lattice of photonic resonators consisting of two types of single-mode cavities. The nearest neighbours are coupled through time-domain modulations, with horizontal phases increasing linearly in y; this breaks T. **d**, An array of helical photonic waveguides, breaking z symmetry, induces harmonic modulations on any photons propagating through it.

Weyl points and line nodes: Towards 3D topological phases

2D Dirac points are the key bandstructures that led to the first proposal and experiments of the photonic analogue of the quantum Hall effect. For 3D[61,62] topological phases, the key bandstructures are line nodes[63], 3D Dirac points[64] and, more fundamentally, Weyl points[65]. However, Weyl points have not yet been realized in nature. Recently, Lu *et al.* theoretically proposed[12] the use of germanium or high-index glass for achieving both line nodes and Weyl points in gyroid photonic crystals at infrared wavelengths.

A line node[63] is a linear line-degeneracy: two bands touch at a closed loop (Fig. 5a) while being linearly dispersed in the other two directions, thus making it the extension of Dirac cone dispersions in three dimensions. For example, $H(\mathbf{k}) = v_x k_x \sigma_x + v_y k_y \sigma_z$ describes a line node along k_z. PT therefore protects both Dirac cones and line nodes. The line node bandstructure in Fig. 5b is found in a double gyroid (DG) photonic crystal with both P and T. The surface dispersions of a line-node photonic crystal can be flat bands in controlled areas of the 2D surface Brillouin zone. When PT is broken, a line node can either open up a gap or split into Weyl points. Figure 5c shows a phase diagram of the DG photonic crystals, where the line node splits into one or two pairs of Weyl points under T or P breaking, respectively.

A Weyl point[65] is a linear point-degeneracy: two bands touch at a single point (Fig. 5d) while being linearly dispersed in all three directions. The low-frequency Hamiltonian of a Weyl point is $H(\mathbf{k}) = v_x k_x \sigma_x + v_y k_y \sigma_y + v_z k_z \sigma_z$. Diagonalization leads to the solution $\omega(\mathbf{k}) = \pm\sqrt{(v_x^2 k_x^2 + v_y^2 k_y^2 + v_z^2 k_z^2)}$. Because all three Pauli matrices are used in the Hamiltonian, the solution cannot have a frequency gap. The existence of the imaginary σ_y term means that breaking PT is a necessary condition for obtaining Weyl points. Weyl points are monopoles of Berry flux (Fig. 5d): a closed surface in a 3D Brillouin zone containing a single Weyl point has a non-zero Chern number of ±1. This means a single Weyl point is absolutely robust in 3D momentum space, as Weyl points must be generated and annihilated pairwise with opposite Chern numbers. When only P is broken (T preserved), the minimum number of pairs of Weyl points is two because T maps a Weyl point at k to $-k$ without changing its Chern number. When only T is broken (P preserved), the minimum number of pairs of Weyl points is one. The bandstructure in Fig. 5e, which contains the minimum of four Weyl points, is realized in a DG photonic crystal under P-breaking. Note that a Dirac point in three dimensions[64] is a linear point-degeneracy between four bands, consisting of two Weyl points of opposite Chern numbers sitting on top of each other in frequency.

A photonic crystal that contains frequency-isolated Weyl points has gapless surface states. Consider the brown plane in the bulk Brillouin zone of Fig. 5f: it encloses either the top red Weyl point ($C = +1$) or the lower three Weyl points, depending on the choice of direction. Either way, this plane has a non-zero Chern number, similar to the 2D Brillouin zone in the quantum Hall case. Thus, any surface state with this particular fixed k_y is gapless and unidirectional.

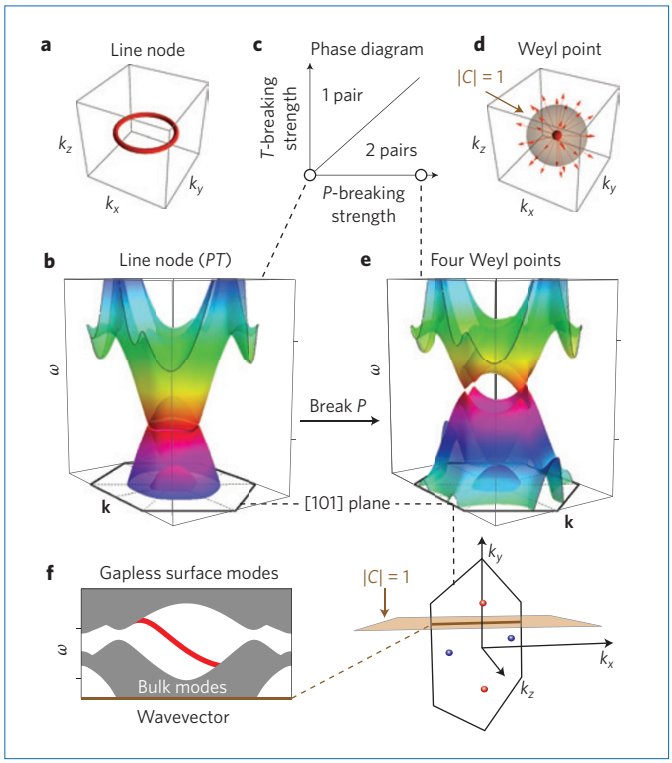

Figure 5 | Phase diagram of line nodes and Weyl points in gyroid photonic crystals. a, Isofrequency line (red) of a line node in 3D momentum space. **b**, The line-node bandstructure of a particular *PT*-symmetric DG photonic crystal. **c**, The phase diagram of 3D linear degeneracies under *T* and *P* breaking perturbations. One and two pairs of Weyl points are the minimum numbers in the *T*- and *P*-dominated phases, respectively. Line nodes are protected when both symmetry-breaking strengths are zero. **d**, An illustration of a Weyl point carrying a Chern number of one. A Weyl point is the source or drain of Berry curvatures (red arrows). **e**, The Weyl point bandstructure of a *P*-broken DG photonic crystal. **f**, Right: a plane in the 3D Brillouin zone that encloses unpaired Weyl points has non-zero Chern numbers. The red and blue colours indicate the opposite Chern numbers of the Weyl points. Left: the surface states associated with this plane have protected gapless dispersions.

Plotted on the left of Fig. 5f is an example of such surface states for the *P*-broken DG photonic crystal.

Outlook

The field of topological photonics has grown exponentially in recent years. Non-trivial topological effects have been proposed and realized across a variety of photonic systems at different wavelengths and in all three spatial dimensions. This Review has introduced the main concepts, experiments and proposals of topological photonics, focusing on 2D and 3D realizations. 1D examples are discussed in refs 66–72.

Over the coming years, we expect the discovery of new topological mirrors, phases and invariants, which could be classified with respect to different symmetries[73–77]. The topological phases of interacting photons[78–80] could be explored by considering nonlinearity[81] and entanglement. Various topologically protected interfacial states between different topological mirrors will be studied. The immunity to disorder and Anderson localization of those interfacial states must be addressed. Moreover, the concepts and realizations of topological photonics can be translated to other bosonic systems such as surface plasmons[70,71], excitons[82], exciton–polaritons[83,84], phonons[85,86] and magnons[87]. Certain other robust wave phenomena can be explained through topological interpretations[88].

Technologically, the exploitation of topological effects could dramatically improve the robustness of photonic devices in the presence of imperfections. As a result, it will become easier to design robust devices. For example, designers will soon worry less about insertion loss and Fabry–Pérot noise due to back-reflections. Topologically protected transport could solve the key limitation from disorder and localization in slow light[35] and in coupled resonator optical waveguides[38]. Unidirectional waveguides could decrease the power requirements of classical signals and improve coherence in quantum links[89,90]. One-way edge states of *T*-breaking topological phases could be used as compact optical isolators[91]. Edge states of *T*-invariant topological phases[11,58] do not have reflection even when the system is reciprocal; thus, isolators may be unnecessary for photonic circuits comprising *T*-invariant topological phases. The realization of practical, topologically protected unidirectional waveguides at optical frequencies is currently the main challenge of this emerging field. Much like the field of topological insulators in electronics, topological photonics promises an enormous variety of breakthroughs in both fundamental physics and technological outcomes.

Received 24 May 2014; accepted 18 September 2014; published online 26 October 2014

References

1. Hasan, M. Z. & Kane, C. L. Colloquium: Topological insulators. *Rev. Mod. Phys.* **82,** 3045–3067 (2010).
2. Qi, X.-L. & Zhang, S.-C. Topological insulators and superconductors. *Rev. Mod. Phys.* **83,** 1057–1110 (2011).
3. Haldane, F. D. M. Model for a quantum Hall effect without landau levels: Condensed-matter realization of the 'parity anomaly'. *Phys. Rev. Lett.* **61,** 2015–2018 (1988).
4. Haldane, F. D. M. & Raghu, S. Possible realization of directional optical waveguides in photonic crystals with broken time-reversal symmetry. *Phys. Rev. Lett.* **100,** 013904 (2008).
5. Raghu, S. & Haldane, F. D. M. Analogs of quantum-Hall-effect edge states in photonic crystals. *Phys. Rev. A* **78,** 033834 (2008).
6. Joannopoulos, J. D., Johnson, S. G., Winn, J. N. & Meade, R. D. *Photonic Crystals: Molding the Flow of Light* 2nd edn (Princeton Univ. Press, 2008).
7. Wang, Z., Chong, Y. D., Joannopoulos, J. D. & Marin Soljačić. Reflection-free one-way edge modes in a gyromagnetic photonic crystal. *Phys. Rev. Lett.* **100,** 013905 (2008).
8. Wang, Z., Chong, Y., Joannopoulos, J. D. & Soljačić., M. Observation of unidirectional backscattering-immune topological electromagnetic states. *Nature* **461,** 772–775 (2009).
9. Hafezi, M., Demler, E. A., Lukin, M. D. & Taylor, J. M. Robust optical delay lines with topological protection. *Nature Phys.* **7,** 907–912 (2011).
10. Fang, K., Yu, Z. & Fan, S. Realizing effective magnetic field for photons by controlling the phase of dynamic modulation. *Nature Photon.* **6,** 782–787 (2012).
11. Khanikaev, A. B. *et al.* Photonic topological insulators. *Nature Mater.* **12,** 233–239 (2013).
12. Lu, L., Fu, L., Joannopoulos, J. D. & Soljačić, M. Weyl points and line nodes in gyroid photonic crystals. *Nature Photon.* **7,** 294–299 (2013).
13. Skirlo, S. A., Lu, L. & Soljačić, M. Multimode one-way waveguides of large Chern numbers. *Phys. Rev. Lett.* **113,** 113904 (2014).
14. Kraus, Y. E., Lahini, Y., Ringel, Z., Verbin, M. & Zilberberg, O. Topological states and adiabatic pumping in quasicrystals. *Phys. Rev. Lett.* **109,** 106402 (2012).
15. Rechtsman, M. C. *et al.* Photonic Floquet topological insulators. *Nature* **496,** 196–200 (2013).
16. Hafezi, M., Mittal, S., Fan, J., Migdall, A. & Taylor, J. M. Imaging topological edge states in silicon photonics. *Nature Photon.* **7,** 1001–1005 (2013).
17. Sepkhanov, R. A., Nilsson, J. & Beenakker, C. W. J. Proposed method for detection of the pseudospin-1/2 Berry phase in a photonic crystal with a Dirac spectrum. *Phys. Rev. B* **78,** 045122 (2008).
18. Sepkhanov, R. A., Ossipov, A. & Beenakker, C. W. J. Extinction of coherent backscattering by a disordered photonic crystal with a Dirac spectrum. *Europhys. Lett.* **85,** 14005 (2009).
19. Peleg, O. *et al.* Conical diffraction and gap solitons in honeycomb photonic lattices. *Phys. Rev. Lett.* **98,** 103901 (2007).

20. Bahat-Treidel, O. *et al.* Klein tunneling in deformed honeycomb lattices. *Phys. Rev. Lett.* **104,** 063901 (2010).
21. Rechtsman, M. C. *et al.* Strain-induced pseudomagnetic field and photonic landau levels in dielectric structures. *Nature Photon.* **7,** 153–158 (2013).
22. Schomerus, H. & Halpern, N. Y. Parity anomaly and Landau-level lasing in strained photonic honeycomb lattices. *Phys. Rev. Lett.* **110,** 013903 (2013).
23. Rechtsman, M. C. *et al.* Topological creation and destruction of edge states in photonic graphene. *Phys. Rev. Lett.* **111,** 103901 (2013).
24. Onoda, M., Murakami, S. & Nagaosa, N. Hall effect of light. *Phys. Rev. Lett.* **93,** 083901 (2004).
25. Ochiai, T. & Onoda, M. Photonic analog of graphene model and its extension: Dirac cone, symmetry, and edge states. *Phys. Rev. B* **80,** 155103 (2009).
26. Fang, K., Yu, Z. & Fan, S. Microscopic theory of photonic one-way edge mode. *Phys. Rev. B* **84,** 075477 (2011).
27. Poo, Y., Wu, R.-X., Lin, Z., Yang, Y. & Chan, C. T. Experimental realization of self-guiding unidirectional electromagnetic edge states. *Phys. Rev. Lett.* **106,** 93903 (2011).
28. Liu, K., Shen, L. & He, S. One-way edge mode in a gyromagnetic photonic crystal slab. *Opt. Lett.* **37,** 4110–4112 (2012).
29. Asatryan, A. A., Botten, L. C., Fang, K., Fan, S. & McPhedran, R. C. Local density of states of chiral Hall edge states in gyrotropic photonic clusters. *Phys. Rev. B* **88,** 035127 (2013).
30. He, C. *et al.* Tunable one-way cross-waveguide splitter based on gyromagnetic photonic crystal. *Appl. Phys. Lett.* **96,** 111111 (2010).
31. Zang, X. & Jiang, C. Edge mode in nonreciprocal photonic crystal waveguide: manipulating the unidirectional electromagnetic pulse dynamically. *J. Opt. Soc. Am. B* **28,** 554–557 (2011).
32. Fu, J.-X., Liu, R.-J. & Li, Z.-Y. Robust one-way modes in gyromagnetic photonic crystal waveguides with different interfaces. *Appl. Phys. Lett.* **97,** 041112 (2010).
33. Fu, J.-X., Lian, J., Liu, R.-J., Gan, L. & Li, Z.-Y. Unidirectional channel-drop filter by one-way gyromagnetic photonic crystal waveguides. *Appl. Phys. Lett.* **98,** 211104 (2011).
34. Qiu, W., Wang, Z. & Soljačić, M. Broadband circulators based on directional coupling of one-way waveguides. *Opt. Express* **19,** 22248–22257 (2011).
35. Yang, Y., Poo, Y., Wu, R.-X., Gu, Y. & Chen, P. Experimental demonstration of one-way slow wave in waveguide involving gyromagnetic photonic crystals. *Appl. Phys. Lett.* **102,** 231113 (2013).
36. Chong, Y. D., Wen, X. G. & Soljačić, M. Effective theory of quadratic degeneracies. *Phys. Rev. B* **77,** 235125 (2008).
37. Yu, Z., Veronis, G., Wang, Z. & Fan, S. One-way electromagnetic waveguide formed at the interface between a plasmonic metal under a static magnetic field and a photonic crystal. *Phys. Rev. Lett.* **100,** 23902 (2008).
38. Mittal, S. *et al.* Topologically robust transport of photons in a synthetic gauge field. *Phys. Rev. Lett.* **113,** 087403 (2014).
39. Umucalılar, R. O. & Carusotto, I. Artificial gauge field for photons in coupled cavity arrays. *Phys. Rev. A* **84,** 043804 (2011).
40. Petrescu, A., Houck, A. A. & Le Hur, K. Anomalous Hall effects of light and chiral edge modes on the Kagome lattice. *Phys. Rev. A* **86,** 053804 (2012).
41. Hafezi, M. Measuring topological invariants in photonic systems. *Phys. Rev. Lett.* **112,** 210405 (2014).
42. Liang, G. Q. & Chong, Y. D. Optical resonator analog of a two-dimensional topological insulator. *Phys. Rev. Lett.* **110,** 203904 (2013).
43. Pasek, P. & Chong, Y. D. Network models of photonic Floquet topological insulators. *Phys. Rev. B* **89,** 075113 (2013).
44. Fang, K., Yu, Z. & Fan, S. Photonic Aharonov–Bohm effect based on dynamic modulation. *Phys. Rev. Lett.* **108,** 153901 (2012).
45. Li, E., Eggleton, B. J., Fang, K. & Fan, S. Photonic Aharonov–Bohm effect in photon–phonon interactions. *Nature Commun.* **5,** 3225 (2014).
46. Tzuang, L. D., Fang, K., Nussenzveig, P., Fan, S. & Lipson, M. Non-reciprocal phase shift induced by an effective magnetic flux for light. *Nature Photon.* **8,** 701–705 (2014).
47. Kitagawa, T., Berg, E., Rudner, M. & Demler, E. Topological characterization of periodically driven quantum systems. *Phys. Rev. B* **82,** 235114 (2010).
48. Lindner, N. H., Refael, G. & Galitski, V. Floquet topological insulator in semiconductor quantum wells. *Nature Phys.* **7,** 490–495 (2011).
49. Kopp, V. I. *et al.* Chiral fiber gratings. *Science* **305,** 74–75 (2004).
50. Jia, S. & Fleischer, J. W. Nonlinear light propagation in rotating waveguide arrays. *Phys. Rev. A* **79,** 041804 (2009).
51. Dalibard, J., Gerbier, F., Juzeliūnas, G. & Öhberg, P. Colloquium: Artificial gauge potentials for neutral atoms. *Rev. Mod. Phys.* **83,** 1523 (2011).
52. Jaksch, D. & Zoller, P. Creation of effective magnetic fields in optical lattices: the Hofstadter butterfly for cold neutral atoms. *New J. Phys.* **5,** 56 (2003).
53. Schmidt, M., Peano, V. & Marquardt, F. Optomechanical metamaterials: Dirac polaritons, gauge fields, and instabilities. Preprint at http://lanl.arxiv.org/abs/1311.7095 (2013).
54. Jia, N., Sommer, A., Schuster, D. & Simon, J. Time reversal invariant topologically insulating circuits. Preprint at http://lanl.arxiv.org/abs/1309.0878 (2013).
55. Kong, J. A. Theorems of bianisotropic media. *Proc. IEEE* **60,** 1036–1046 (1972).
56. Jonsson, F. & Flytzanis, C. Photospin-orbit coupling in photonic structures. *Phys. Rev. Lett.* **97,** 193903 (2006).
57. Ma, T., Khanikaev, A. B., Mousavi, S. H. & Shvets, G. Topologically protected photonic transport in bi-anisotropic meta-waveguides. Preprint at http://lanl.arxiv.org/abs/1401.1276 (2014).
58. Chen, W.-J., Jiang, S.-J., Chen, X.-D., Dong, J.-W. & Chan, C. T. Experimental realization of photonic topological insulator in a uniaxial metacrystal waveguide. Preprint at http://lanl.arxiv.org/abs/1401.0367 (2014).
59. Gao, W. *et al.* Chiral hyperbolic metamaterial as a robust photonic topological insulator. Preprint at http://lanl.arxiv.org/abs/1401.5448 (2014).
60. Kraus, Y. E., Ringel, Z. & Zilberberg, O. Four-dimensional quantum Hall effect in a two-dimensional quasicrystal. *Phys. Rev. Lett.* **111,** 226401 (2013).
61. Chen, W.-J. *et al.* Observation of backscattering-immune chiral electromagnetic modes without time reversal breaking. *Phys. Rev. Lett.* **107,** 023901 (2011).
62. Lu, L., Joannopoulos, J. D. & Soljačić, M. Waveguiding at the edge of a three-dimensional photonic crystal. *Phys. Rev. Lett.* **108,** 243901 (2012).
63. Burkov, A. A., Hook, M. D. & Balents, L. Topological nodal semimetals. *Phys. Rev. B* **84,** 235126 (2011).
64. Young, S. M. *et al.* Dirac semimetal in three dimensions. *Phys. Rev. Lett.* **108,** 140405 (2012).
65. Wan, X., Turner, A. M., Vishwanath, A. & Savrasov, S. Y. Topological semimetal and Fermi-arc surface states in the electronic structure of pyrochlore iridates. *Phys. Rev. B* **83,** 205101 (2011).
66. Malkova, N., Hromada, I., Wang, X., Bryant, G. & Chen, Z. Observation of optical Shockley-like surface states in photonic superlattices. *Opt. Lett.* **34,** 1633–1635 (2009).
67. Tan, W., Sun, Y., Chen, H. & Shen, S.-Q. Photonic simulation of topological excitations in metamaterials. *Sci. Rep.* **4,** 3842 (2014).
68. Poshakinskiy, A. V., Poddubny, A. N., Pilozzi, L. & Ivchenko, E. L. Radiative topological states in resonant photonic crystals. *Phys. Rev. Lett.* **112,** 107403 (2014).
69. Xiao, M., Zhang, Z. Q. & Chan, C. T. Surface impedance and bulk band geometric phases in one-dimensional systems. *Phys. Rev. X* **4,** 021017 (2014).
70. Poddubny, A., Miroshnichenko, A., Slobozhanyuk, A. & Kivshar, Y. Topological Majorana states in zigzag chains of plasmonic nanoparticles. *ACS Photon.* **1,** 101–105 (2014).
71. Ling, C. W., Xiao, M., Yu, S. F. & Fung, K. H. Topological edge plasmon modes between diatomic chains of nanoparticles. Preprint at http://lanl.arxiv.org/abs/1401.7520 (2014).
72. Poli, C., Bellec, M., Kuhl, U., Mortessagne, F. & Schomerus, H. Selective enhancement of topologically induced interface states. Preprint at http://lanl.arxiv.org/abs/1407.3703 (2014).
73. Kitaev, A. Periodic table for topological insulators and superconductors. *AIP Conf. Proc.* **1134,** 22 (2009).
74. Schnyder, A. P., Ryu, S., Furusaki, A. & Ludwig, A. W. W. Classification of topological insulators and superconductors in three spatial dimensions. *Phys. Rev. B* **78,** 195125 (2008).
75. Fu, L. Topological crystalline insulators. *Phys. Rev. Lett.* **106,** 106802 (2011).
76. Yannopapas, V. Gapless surface states in a lattice of coupled cavities: A photonic analog of topological crystalline insulators. *Phys. Rev. B* **84,** 195126 (2011).
77. De Nittis, G. & Lein, M. On the role of symmetries in the theory of photonic crystals. *Ann. Phys.* **350,** 568–587 (2014).
78. Chen, X., Gu, Z.-C., Liu, Z.-X. & Wen, X.-G. Symmetry-protected topological orders in interacting bosonic systems. *Science* **338,** 1604–1606 (2012).
79. Umucalilar, R. O. & Carusotto, I. Fractional quantum Hall states of photons in an array of dissipative coupled cavities. *Phys. Rev. Lett.* **108,** 206809 (2012).
80. Hafezi, M., Lukin, M. D. & Taylor, J. M. Non-equilibrium fractional quantum Hall state of light. *New J. Phys.* **15,** 063001 (2013).
81. Lumer, Y., Plotnik, Y., Rechtsman, M. C. & Segev, M. Self-localized states in photonic topological insulators. *Phys. Rev. Lett.* **111,** 243905 (2013).
82. Yuen-Zhou, J., Saikin, S. K., Yao, N. Y. & Aspuru-Guzik, A. Topologically protected excitons in porphyrin thin films. *Nature Mater.* http://dx.doi.org/10.1038/nmat4073 (2014).
83. Jacqmin, T. *et al.* Direct observation of Dirac cones and a flatband in a honeycomb lattice for polaritons. *Phys. Rev. Lett.* **112,** 116402 (2014).
84. Karzig, T., Bardyn, C.-E., Lindner, N. & Refael, G. Topological polaritons from quantum wells in photonic waveguides or microcavities. Preprint at http://lanl.arxiv.org/abs/1406.4156 (2014).
85. Prodan, E. & Prodan, C. Topological phonon modes and their role in dynamic instability of microtubules. *Phys. Rev. Lett.* **103,** 248101 (2009).

86. Kane, C. L. & Lubensky, T. C. Topological boundary modes in isostatic lattices. *Nature Phys.* **10,** 39–45 (2013).
87. Shindou, R., Matsumoto, R. & Murakami, S. Topological chiral magnonic edge mode in a magnonic crystal. *Phys. Rev. B* **87,** 174427 (2013).
88. Zhen, B., Hsu, C. W., Lu, L., Stone, A. D. & Soljačić, M. Topological nature of bound states in the radiation continuum. Preprint at http://lanl.arxiv.org/abs/1408.0237 (2014).
89. Koch, J., Houck, A. A., Le Hur, K. & Girvin, S. M. Time-reversal-symmetry breaking in circuit-QED-based photon lattices. *Phys. Rev. A* **82,** 043811 (2010).
90. Aspuru-Guzik, A., Demler, E. & White, A. G. Observation of topologically protected bound states in photonic quantum walks. *Nature Commun.* **3,** 882 (2012).
91. Jalas, D. *et al.* What is and what is not an optical isolator. *Nature Photon.* **7,** 579–582 (2013).
92. Nakahara, M. *Geometry, topology, and physics* (CRC, 2003).
93. Xiao, D., Chang, M.-C. & Niu, Q. Berry phase effects on electronic properties. *Rev. Mod. Phys.* **82,** 1959 (2010).
94. Fukui, T., Hatsugai, Y. & Suzuki, H. Chern numbers in discretized Brillouin zone: Efficient method of computing (spin) Hall conductances. *J. Phys. Soc. Japan* **74,** 1674–1677 (2005).
95. Pancharatnam, S. Generalized theory of interference, and its applications. *Proc. Indiana Acad. Sci.* **A44,** 247–262 (1956).
96. Berry, M. V. Quantal phase factors accompanying adiabatic changes. *Proc. R. Soc. Lond A* **392,** 45–57 (1984).
97. Tomita, A. & Chiao, R. Y. Observation of Berry's topological phase by use of an optical fiber. *Phys. Rev. Lett.* **57,** 937 (1986).
98. Kane, C. L. & Mele, E. J. Z2 topological order and the quantum spin Hall effect. *Phys. Rev. Lett.* **95,** 146802 (2005).

Acknowledgements

L.L. thanks L. Fu, C. Wang and A. Khanikaev for discussions. The authors thank P. Rebusco and C.W. Hsu for critical reading and editing of the manuscript. J.J. was supported in part by the U.S.A.R.O. through the ISN, under contract W911NF-07-D-0004. L.L. was supported in part by the MRSEC Program of the NSF under award DMR-0819762. M.S. and L.L. were supported in part by the MIT S3TEC EFRC of DOE under grant DE-SC0001299.

Author contributions

All authors contributed equally to this work.

Additional information

Reprints and permissions information is available online at www.nature.com/reprints. Correspondence and requests for materials should be addressed to L.L.

Competing financial interests

The authors declare no competing financial interests.